

Dissociative recombination of N_2H^+

S. Fonseca dos Santos, V. Ngassam, and A. E. Orel

Department of Chemical Engineering, University of California, Davis, California 95616, USA

Å. Larson*

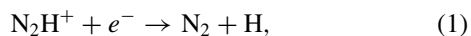
Department of Physics, Stockholm University, SE-106 91 Stockholm, Sweden

(Received 20 May 2016; published 5 August 2016)

The direct and indirect mechanisms of dissociative recombination of N_2H^+ are theoretically studied. At low energies, the electron capture is found to be driven by recombination into bound Rydberg states, while at collision energies above 0.1 eV, the direct capture and dissociation along electronic resonant states becomes important. Electron-scattering calculations using the complex Kohn variational method are performed to obtain the scattering matrix as well as energy positions and autoionization widths of resonant states. Potential-energy surfaces of electronic bound states of N_2H and N_2H^+ are computed using structure calculations with the multireference configuration interaction method. The cross section for the indirect mechanism is calculated using a vibrational frame transformation of the elements of the scattering matrix at energies just above the ionization threshold. Here vibrational excitations of the ionic core from $v = 0$ to $v = 1$ and $v = 2$ for all three normal modes are considered and autoionization is neglected. The cross section for the direct dissociation along electronic resonant states is computed with wave-packet calculations using the multiconfiguration time-dependent Hartree method, where all three internal degrees of freedom are considered. The calculated cross sections are compared to measurements.

DOI: [10.1103/PhysRevA.94.022702](https://doi.org/10.1103/PhysRevA.94.022702)**I. INTRODUCTION**

Dissociative recombination (DR) of N_2H^+ is a reaction important for the understanding of the chemistry of the interstellar medium. The N_2H^+ ion has been detected in numerous astrophysical environments [1–6] and it is used to model the density of nitrogen, which lacks observable vibrational or rotational transitions. N_2H^+ is formed by proton transfer in collisions of N_2 and H_3^+ and it is destroyed by dissociative recombination with low-energy electrons



where all nitrogen is recycled. This reaction has gained substantial attention both experimentally [7–13] and theoretically [14–18].

DR measurements of this reaction have been performed using both the Flowing Afterglow Langmuir Probe technique [7,8,10–12] and ion-storage ring experiments [9,13]. They now agree on a relative large thermal rate coefficient of about $2.7 \times 10^{-7} \text{ cm}^3\text{s}^{-1}$ and a dominance of breakup into $\text{N}_2 + \text{H}$ [11–13].

Extensive theoretical studies of the potential-energy surfaces of electronic states of $^2A'$ symmetry important for the DR reaction have been carried out by the group of Talbi and Hickman [14–16,18]. In [14] structure calculations were performed at linear geometries with the NN distance frozen, using the multireference configuration-interaction (MRCI) method with orbitals of localized character. Quasidiabatic states were generated by analyzing the configurations of the electronic states. Two repulsive resonant states were found, but the potentials of these states cross the ion potential at internuclear distances larger than outer classical turning point of the vibrational $v = 0$ wave function of the ion. Therefore,

it was concluded that the direct DR cross section through these resonant states should be small for vibrationally relaxed ions.

In the following publications [15,16,18], the block-diagonalization method [19] was used to generate slices of potential-energy surfaces of diabatic resonant states. In [15], the NN distance was frozen at the equilibrium value of the N_2H^+ ion, while the potential-energy surface of the lowest electronic resonant state was computed as a function of the other two Jacobi coordinates. Two-dimensional wave-packet calculations were carried out using the MCTDH [20] (multiconfiguration time-dependent Hartree) program package. In this study, no information about the autoionization width of the resonant state was known. Therefore, it was assumed that the width has a small magnitude and is constant (independent of the nuclear coordinates). Autoionization was thus neglected and the absolute cross section was not computed. The calculated relative cross section shows a peak centered around 3 eV with a negligible contribution to the cross section at low energies [15]. This was followed by a study [16], where also the NN dependencies of the resonant states were examined. The potential-energy surfaces of the lowest two resonant states of $^2A'$ symmetry were found to be repulsive in the Franck-Condon region. These studies conclude that the indirect mechanism might be important in N_2H^+ DR.

In a previous study [17], the indirect dissociative recombination of N_2H^+ was investigated using a vibrational frame transformation of the elements of the elastic scattering matrix computed using electron-scattering calculations with the complex-Kohn variational method [21]. The indirect DR cross section was calculated by assuming that the electron is captured into bound Rydberg states when the ionic core is vibrationally excited from $v = 0$ to $v = 1$. The quantum defects obtained using electron-scattering calculations were compared with those calculated from converged bound Rydberg states obtained with structure calculations. For the vibrational wave

*aasal@fysik.su.se

functions, harmonic-oscillator wave functions were used and the effect of autoionization was neglected. The model assumed linear dependence of the elements of the scattering matrix as functions of the normal-mode coordinates.

Here, we present an independent study of the electronic states important in the N_2H^+ dissociative recombination. Electronic-structure calculations using the MRCI method are combined with electron-scattering calculations using the complex-Kohn variational method [21]. We thus obtain not only potential-energy surfaces, but also autoionization widths as well as the electron-scattering matrix. The indirect DR cross section is again calculated using a vibrational frame transformation of the scattering matrix elements. However, present treatment includes both vibrational excitation from $v = 0$ to $v = 1$ and 2 and up to quadratic dependence of the elements of the scattering matrix is considered. The contribution to the cross section from direct DR is computed using wave-packet propagation on quasidiabatic resonant-state potentials including all three degrees of freedom using the MCTDH program package.

The outline of this paper is as follows. In Sec. II, the theoretical models of the indirect and direct DR mechanisms are described. This is followed in Sec. III by a description of the computational details of the electron scattering and structure calculations as well as the wave-packet propagation scheme using the MCTDH technique. The results are presented in Sec. IV, where the potential-energy surfaces of the resonant states are compared with previously calculated surfaces and the computed DR cross sections are compared with measurements. We discuss the role of the two mechanisms and the importance of including all degrees of freedom in the study of the nuclear dynamics. Unless otherwise stated, atomic units are used throughout.

II. THEORETICAL APPROACH

Here we separately study the indirect and direct mechanisms of N_2H^+ DR. As described below, the two processes are studied using simplified models and no interference effects between the two electron-capture mechanisms are considered. Additionally, no electronic couplings between the resonant states and the Rydberg manifold converging to the ionic ground state are included.

A. Indirect mechanism

The simplified model for the indirect DR mechanism has been previously described and applied to compute the DR cross section for numerous polyatomic ions [17,22,23]. The model is based on the basic assumptions that the electron capture goes through the bound Rydberg states causing the ionic core to be vibrationally excited. Rotation is not included and it is assumed that as soon as the electron is captured, the system will predissociate with zero probability for autoionization. By averaging the cross section over autoionizing resonances, a constant electron-capture probability is obtained. Additionally, the harmonic-oscillator approximation is used for describing the vibrational wave function of the ionic core. Using these approximations, the indirect DR cross section at the collision

energy E can be estimated with the simple formula

$$\sigma = \frac{\pi}{2E} \sum_{\substack{\Lambda \ v_n \\ lm'l'm'}} g_{\Lambda} |\langle \chi_0 | S_{lm'l'm'}^{\Lambda} | \chi_{v_n} \rangle|^2 [1 - \theta(E - E_{v_n})], \quad (2)$$

where χ_{v_n} and χ_0 are the final and initial vibrational wave functions of the ionic core and $S_{lm,l'm'}^{\Lambda}$ is an element of the elastic-scattering matrix in overall symmetry Λ just above the ionization threshold (in an energy region where there are no contributions from electronic resonant states). In the expression above, l, m, l', m' label the incoming and outgoing angular momentum quantum numbers of the scattered electron and g_{Λ} is the multiplicity ratio for the given electronic symmetry. The factor involving the Heaviside step function, $[1 - \theta]$, guarantees that the contribution to the cross section becomes zero when the electronic energy is greater than the corresponding vibrational threshold, E_{v_n} . The summations run over the final vibrational state of the ionic core as well as all elements of the scattering matrix. The model has previously been applied to compute the indirect DR cross section of N_2H^+ [17] for vibrational excitation from $v = 0$ to $v = 1$ for the three normal modes of the ionic core. Here the model is extended to also include excitations from $v = 0$ to $v = 2$. This is done by fitting the elements of the scattering matrix to second-order polynomials as functions of the normal-mode coordinates and using harmonic-oscillator wave functions for the vibrational wave functions to obtain analytical expressions for the matrix elements $\langle \chi_0 | S_{lm'l'm'}^{\Lambda} | \chi_{v_n} \rangle$.

B. Direct mechanism

As described below, the potential-energy surfaces of the quasidiabatic electronic resonant states of N_2H are computed by combining electron-scattering and structure calculations. Autoionization widths and energy positions of the resonant states are obtained from the electron-scattering calculations. Here no couplings (electronic nor nonadiabatic) among the neutral states are considered, but it is assumed that electron capture into the resonant state may either lead to autoionization or dissociation along the potential-energy surface. The potential-energy surfaces $[V_i(\mathbf{R})]$ and autoionization widths $[\Gamma_i(\mathbf{R})]$ are calculated using Jacobi coordinates (see Fig. 1), where all three degrees of freedom $[\mathbf{R} = (r, z, \theta)]$ are considered.

The nuclear dynamics is studied using a wave-packet propagation scheme, where the time-dependent Schrödinger equation is numerically solved

$$i \frac{\partial}{\partial t} \Psi_i(t, \mathbf{R}) = \left[\hat{T} + V_i(\mathbf{R}) - i \frac{1}{2} \Gamma_i(\mathbf{R}) \right] \Psi_i(t, \mathbf{R}). \quad (3)$$

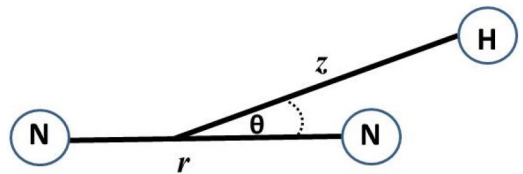


FIG. 1. Jacobi coordinates used in the wave-packet propagation scheme. The radial coordinates are denoted by r and z and the Jacobi angle by θ .

Autoionization is here included using the local approximation [24,25], where it is assumed that the total energy of the system is high enough for autoionization into a complete set of vibrational levels. Zero angular momentum of the molecular system is assumed (rotation is neglected) and with the Jacobi coordinates, the nuclear kinetic-energy operator has the form

$$\hat{T} = -\frac{1}{2\mu_r} \frac{\partial^2}{\partial r^2} - \frac{1}{2\mu_z} \frac{\partial^2}{\partial z^2} - \frac{1}{2} \left(\frac{1}{\mu_r r^2} + \frac{1}{\mu_z z^2} \right) \frac{1}{\sin\theta} \frac{\partial}{\partial\theta} \sin\theta \frac{\partial}{\partial\theta}, \quad (4)$$

where μ_r and μ_z are the reduced masses associated with the r and z coordinates.

The wave packets are initiated on the resonant states using the initial condition [24]

$$\Psi_i(t=0, \mathbf{R}) = \sqrt{\frac{\Gamma_i(\mathbf{R})}{2\pi}} \chi_0(\mathbf{R}). \quad (5)$$

Here χ_0 is the vibrational wave function of the N₂H⁺ ion. Electron recombination with ions in their ground vibrational level ($v=0$) is considered. Wave packets are propagated on the complex potential-energy surfaces. At large radial distances, complex absorbing potentials are included. These will prevent wave-packet reflection from the end of the grid and they are used for calculating the DR cross section

$$\sigma_i(E) = \frac{2\pi^3}{E} g_i (|T_{i,r}(E)|^2 + |T_{i,z}(E)|^2). \quad (6)$$

Here g_i is the ratio of multiplicity of the neutral state to the ionization continuum and $|T_{i,x}(E)|^2$ is the transition probability for dissociating in the radial coordinate x . (For more details, see Ref [26].)

III. COMPUTATIONAL DETAILS

A. Electronic-structure calculations

In C_s symmetry, the \tilde{X}^2A' ground state of N₂H has the dominant configuration $(1a')^2(2a')^2(3a')^2(4a')^2(5a')^2(1a'')^2(6a')^2(7a')^1$. The ground state of the ion corresponds to the removal of an electron from the $(7a')$ orbital. Other low-lying ionic states are formed when an electron is removed from the $(1a'')$ orbital leading to the $^1A''$ and $^3A''$ states, and by the removal of an electron from the $(6a')$ orbital resulting in formation of $^1A'$ and $^3A'$ electronic states. The resonances seen in electron scattering from N₂H⁺ are Rydberg states converging to these excited ionic cores. They are crossed at large internuclear separations by Rydberg states converging to even higher excited ionic states.

For the direct DR model, the potential-energy surfaces of the ion as well as excited states of the neutral molecule are calculated using the MRCI method. This will provide us with the potential energy of the electronically bound states that are situated below the ground state of the ion. We also use the structure calculations to interpolate the potentials of the resonant states between the geometries where electron-scattering calculations are performed. Although the ground state of the ion has $C_{\infty v}$ symmetry, as the molecule is bent the symmetry reduces to C_s . Since our calculations include

all three dimensions, the calculations are carried out in C_s symmetry.

In order to describe both the Rydberg series converging to the various excited ionic states, which are the electronic resonances, as well as describing the bound Rydberg states converging to the ground ionic core, we first carry out a self-consistent-field (SCF) calculation on the ground state of the neutral molecule with a basis set consisting of $(4s, 1p)$ primitive functions contracted to $[3s, 1p]$ for the hydrogen and triple-zeta plus polarization basis $(9s, 7p, 1d)$ contracted to $[4s, 4p, 1d]$ for the nitrogen atom. In the next step, these SCF orbitals are used in a MRCI calculation on the ground state of the ion, where the two lowest orbitals ($1a'$) and ($2a'$) mainly composed of the $(1s)$ atomic orbitals on the two nitrogen atoms are frozen and the next eight orbitals form the active space. A full CI is done in the active space and single and double excitations from this set of configurations are allowed into the remaining orbitals. Natural orbitals are obtained from this calculation. The natural orbitals are then further expanded by adding diffuse $(1s, 1p)$ orbitals on nitrogen and $(2s, 2p)$ on hydrogen.

Then a MRCI calculation is carried out to determine the potential-energy surfaces of the ground state of the ion as well as excited states of the neutral molecule. In these calculations, the two lowest ($1a'$) and ($2a'$) core orbitals are kept doubly occupied and the reference configurations are constructed by excitations of eight electrons (seven for the ion) among the seven orbitals: $(3a')$, $(4a')$, $(5a')$, $(6a')$, $(1a'')$, $(7a')$, and $(2a'')$. Single excitations out of the reference configurations are included.

B. Electron-scattering calculations

The energy positions and autoionization widths of the electronic resonant states are determined using the complex-Kohn variational method [21]. The trial wave function for the neutral ($N+1$ electron) system is written as

$$\Psi_{\gamma_0} = \sum_{\gamma} A[\Phi_{\gamma} F_{\gamma\gamma_0}] + \sum_{\mu} d_{\mu}^{\gamma_0} \Theta_{\mu}. \quad (7)$$

The first sum is denoted as the P -space portion of the wave function and runs over the energetically open target states. Here, the symbol index γ labels all quantum numbers representing a physical scattering state (the composite system), and the index γ_0 label the initial state of the target ion. $\Phi_{\gamma}(\mathbf{r}_1, \dots, \mathbf{r}_N; \mathbf{R})$ represents the target wave function for the ion, while the function $F_{\gamma\gamma_0}(\mathbf{r}_{N+1})$ is the one-electron wave function describing the scattered electron. A is an antisymmetrization operator for the electronic coordinates. To obtain consistent structure and scattering calculations, we use the same MRCI target wave function as described in the previous section. The second term, denoted as the Q -space portion of the wave function, contains the functions $\Theta_{\mu}(\mathbf{r}_1, \dots, \mathbf{r}_{N+1}; \mathbf{R})$, which are square-integrable $N+1$ configuration-state functions (CSFs) that are used to describe short-range correlations and the effects of closed channels. We use the same natural orbitals as those applied in the structure calculations as described above. The advantage of using natural orbitals is that the orbital space used to generate these states is kept manageably small. The one-electron scattering

wave function $F_{\gamma\gamma_0}$ is further expanded as

$$F_{\gamma\gamma_0}(\mathbf{r}) = \sum_j c_j^{\gamma\gamma_0} \phi_j + \sum_{lm} [f_l^\gamma \delta_{ll_0} \delta_{mm_0} \delta_{\gamma\gamma_0} + T_{ll_0mm_0}^{\gamma\gamma_0} g_l^\gamma] Y_{lm}(\hat{\mathbf{r}})/r. \quad (8)$$

Here $\phi_j(\mathbf{r})$ are a set of square-integrable functions, and since this is electron-ion scattering, $f_l^\gamma(k_\gamma r)$ and $g_l^\gamma(k_\gamma r)$ are the incoming and outgoing Coulomb functions for a scattered electron with channel momenta k_γ . Y_{lm} are spherical harmonics and angular momenta up to $l = 4$ and $|m| = 4$ are included in the calculation.

By inserting the trial wave function into the complex-Kohn functional [21], the unknown coefficients in the trial wave function can be optimized. Also the T matrix ($T_{ll_0mm_0}^{\gamma\gamma_0}$) for elastic scattering is obtained and by fitting the eigenphase sum of the T matrix to a Breit-Wigner form [27], the energy positions and autoionization widths of the resonant states are determined. These electron-scattering calculations are carried out for a fixed geometry $\mathbf{R} = (r, z, \theta)$ of the target ion.

C. Quasidiabatization

As mentioned above, the ionic ground state is dominated by the following configuration: $(1a')^2(2a'')^2(3a')^2(4a')^2(5a')^2(1a'')^2(6a')^2$. When structure calculations are carried out, three types of states are obtained. These are the Rydberg states converging to the ground ionic core, the states trying to describe the ionization continuum, as well as the resonant states. Both the Rydberg states as well as the states describing the ionization continuum have the same configuration as the ground state of the ion plus an outer electron in a diffuse orbital. The resonant states are more or less compact Rydberg states converging to excited ionic cores. These resonant states all have a vacancy in either the $(1a'')$ or the $(6a')$ orbitals. By identifying the states with these characters, the resonant states can be “diabatized” relative to the Rydberg states and the ionization continuum. This is done in order to follow the resonant states when they cross the ionic ground state and interact with the Rydberg manifold situated below the ionic potential. This approach is also employed to obtain more data for the potential-energy surfaces of the resonant states above the ion and interpolate and extrapolate between the energies of the resonant states calculated using the electron-scattering formalism. It should be noted that this approach will provide us with the energy of the resonant state within the energy spread given by the autoionization width. The resonant states are very narrow, and hence the use of structure data to obtain resonant states is relatively accurate. We have only diabated the resonant states relative to the Rydberg states by using the CI coefficients. We have not calculated any electronic couplings between the neutral states. In addition, we have not diabated the resonant states among each other. As will be shown below, there are clear indications of avoided crossings among the resonant states.

D. Nuclear dynamics

The wave packets are propagated using the MCTDH method described in detail in [28]. Using this program all terms in

the Hamiltonian must be given in a product form. Therefore, calculated potential-energy surfaces of the ion and resonant states as well as the autoionization widths have to be fitted to a product form. The potential-energy surfaces as well as autoionization widths are calculated on a product grid for the (z, θ) Jacobi coordinates when $r = 2.086a_0$. The autoionization widths are also generated on the product grid in (r, z) for fixed $\theta = 1^\circ$. The autoionization widths (Γ_i) (as well as the corresponding functions $\sqrt{\Gamma_i/2\pi}$) are assumed to have the form

$$\Gamma_i(r, z, \theta) = \Gamma_{i,1}(z, \theta) + \Gamma_{i,2}(r, z), \quad (9)$$

where both $\Gamma_{i,1}$ and $\Gamma_{i,2}$ are fitted to the product form using the POTFIT program included in the MCTDH program package [20]. For the potential-energy surfaces of the ion and the resonant states, we assume the form

$$V_i(r, z, \theta) = V_{i,1}(z, \theta) + V_{i,2}(r), \quad (10)$$

where the term $V_{i,1}$ is obtained using POTFIT from the *ab initio* data, while for $V_{i,2}$ describing the dependence on the radial coordinate r (NN distance), the surfaces are fitted to a Morse potential. For the N_2H^+ equilibrium values of z and θ , the potentials are well described by Morse potentials.

The initial vibrational wave function $\chi_0(\mathbf{R})$ of the target ion is computed by using energy relaxation, i.e., propagating the wave packet on the ion potential-energy surface with imaginary time. Here 50 fs is needed to obtain a relaxed wave function. To obtain the initial wave packet on the resonant states [see Eq. (5)], the vibrational wave function is then multiplied by the electronic coupling function between the ionization continuum and the resonant state, $\sqrt{\Gamma_i(\mathbf{R})/2\pi}$.

The nuclear wave packet of N_2H is expressed in the Jacobi coordinates as a sum of products of “single-particle functions” as

$$\Psi_i(t, \mathbf{R}) = \sum_{j=1}^{N_r} \sum_{k=1}^{N_z} \sum_{l=1}^{N_\theta} A_{jkl}(t) \rho_j(t, r) \varrho_k(t, z) \Theta_l(t, \theta). \quad (11)$$

In the present study, 20 single-particle functions are used for each Jacobi coordinate and the single-particle function is expanded in terms of a primitive basis. Here a sine basis with 300 basis functions is applied for the two radial coordinates, while a Legendre basis with 300 functions is used for the angular motion. The time-independent basis functions are chosen as the basis function for a discrete variable representation (DVR). By inserting the expression for the wave function into the time-dependent Schrödinger equation, the time-dependent coupled MCTDH working equations for the coefficients and the single-particle functions can be obtained [28]. The wave packets are propagated using the constant mean-field scheme where the single-particle functions are integrated using the Bulirsch-Stoer extrapolation (BS) scheme of order 7 and an error tolerance of 10^{-6} . For the coefficients, a complex short iterative Lanczos (SIL) algorithm of order 30 is applied, with an error tolerance of 10^{-5} . The wave packets are propagated on the resonant states for 500 fs and the cross section for DR is computed by analyzing the flux absorbed by complex absorbing potentials (CAPs) with strength parameters 0.05 and orders 3, placed at $z = 8.0a_0$ and $r = 4.0a_0$. For all resonant states, we obtain a clear dominance in $\text{N}_2 + \text{H}$

dissociation. That is, the cross sections are composed of mainly flux absorbed by the CAP placed at $z = 8.0a_0$. The total cross section for direct DR is obtained by summarizing the contributions from all resonant states. Here five resonant states of $^2A'$ and $^2A''$ symmetries are included.

IV. RESULTS

The potential-energy surfaces and autoionization widths of quasideiabatic resonant states driving the direct DR of N_2H^+ will be presented. These are compared with the resonant-state potentials calculated by the group of Talbi and Hickman [14–16,18]. The electron-scattering calculation carried out to study the indirect mechanism is slightly different than the one described above. Results from these calculations, such as channel quantum defects, have been presented previously [17] and will not be shown here. The calculated DR cross sections from the direct and indirect mechanisms are compared with the measured cross section.

A. Quasideiabatic resonant states

By carrying out electron-scattering calculations and combining these with the structure calculations, we can extract potential-energy surfaces of the resonant states of N_2H . We calculated five resonant states in each of the $^2A'$ and $^2A''$ symmetries. These are the resonant states with energies below the first excited state of the ion. As described above, the resonant states are diabaticized relative to the Rydberg states converging to the ground ionic core. However, the resonant states are not diabaticized relative to each other. In Fig. 2, we display a comparison between the resonance curves derived from this diabaticization procedure and those obtained from the scattering calculation.

The potential-energy surfaces of the five lowest quasideiabatic resonant states of $^2A'$ and $^2A''$ symmetries are calculated for $z \in [2.0a_0, 10.0a_0]$, $\theta \in [1^\circ, 89^\circ]$ for $r = 2.086a_0$. Since the molecule is symmetric under reflections in $\theta = 0^\circ$ and $\theta = 90^\circ$ (see Fig. 1), the potential-energy surfaces are thus computed for all values of θ . Additionally, the r dependencies of the potentials for $z = 3.0a_0$ and $\theta = 1^\circ$ are determined. One-dimensional slices of the potential-energy surfaces of the ground state of the ion and the five lowest resonant states of $^2A'$ and $^2A''$ symmetries are displayed in Fig. 3. In (a) and (b), some of the asymptotic limits of the lowest resonant states are displayed when the NH bond is broken. These limits are identified by analyzing the configurations of the electronic states and the calculated energies. In agreement with what was found by the group of Talbi [18], the lowest resonant state of $^2A'$ is quasideiabatically dissociating into $\text{N}_2(^3\Sigma_u^+) + \text{H}$. The next $^2A'$ and $^2A''$ are both associated with the $\text{N}_2(^3\Pi_g) + \text{H}$ limit.

The potential-energy surfaces of the resonant states exhibit outer local minimum both when the angle is varied [as can be seen in Figs. 3(c) and 3(d)] and as functions of the NN bond length [as displayed in (e) and (f)]. The minimum in the angular degree arises due to interaction between the resonant states and the Rydberg manifold. The minimum found when the NN bond length is varied is due to the large NN bond dissociation energy and similar minimum is also found for

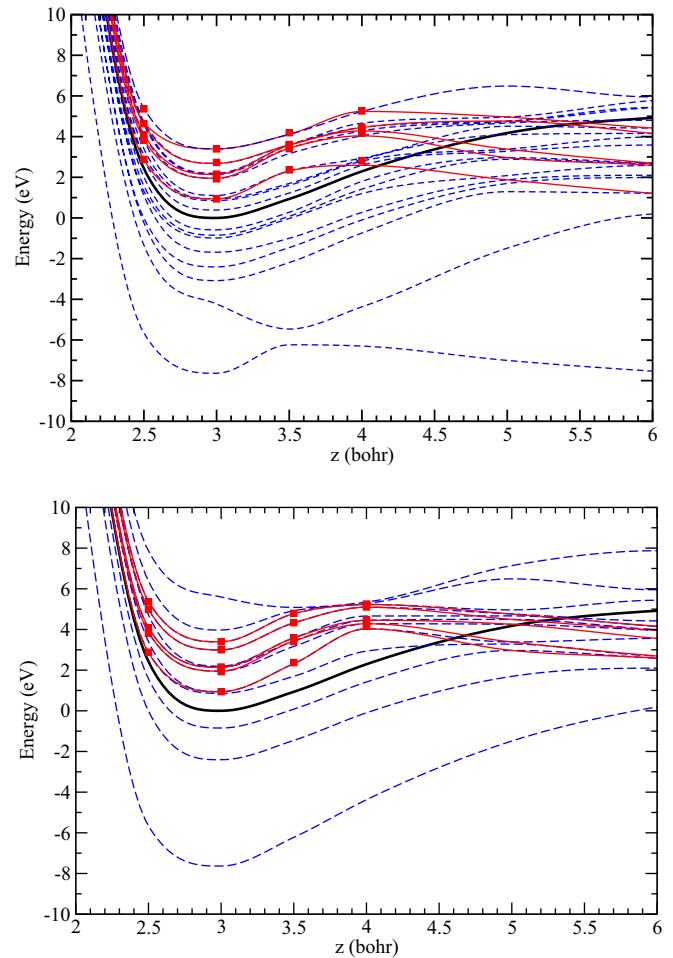


FIG. 2. Potentials of N_2H , top, $^2A'$, bottom, $^2A''$ symmetries are displayed as functions of the z coordinate, while the NN distance $r = 2.086a_0$ and the angle $\theta = 179.0^\circ$ are frozen. Heavy line shows the potential of N_2H^+ ground state, while the dashed lines (blue online) show the potentials of N_2H obtained from the structure calculations. The potential-energy surfaces of the resonant states abstracted using the diabaticization described in the text are shown with solid lines (red online). These are compared to the results of the scattering calculations shown as solid squares (red online).

bound adiabatic states. At low collision energies, the NN bond will not break during the dissociation dynamics.

The electron-scattering calculations will provide us not only with the energy positions of the resonant states, but also with the autoionization widths. In Fig. 4, the one-dimensional cuts of the autoionization widths of the five resonant states of $^2A'$ and $^2A''$ symmetries are displayed. The symbols show the values obtained from the electron-scattering calculations, while lines are splined curves connecting the points. As soon as the potential of the resonant state crosses the ion potential, the autoionization width is put to zero.

As mentioned, there have been previous calculations by the group of Talbi and Hickman [14–16,18] on the potential-energy surfaces of N_2H involved in dissociative recombination. In [16] the calculations were done using the block-diagonalization technique in linear geometry and overall 2A_1 symmetry. Adiabatic and diabatic potential-energy

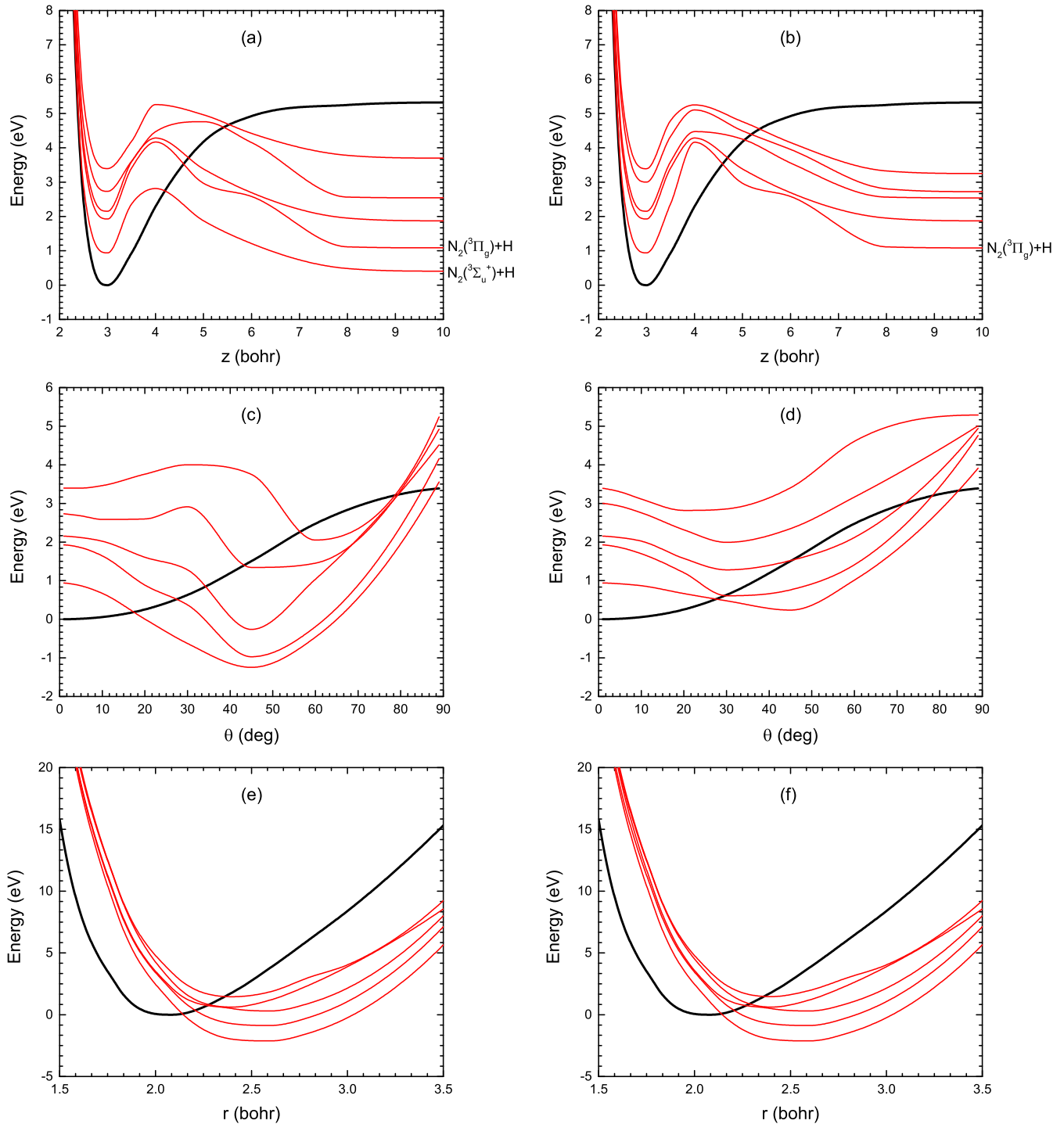


FIG. 3. Resonant-state potential-energy surfaces of N_2H are displayed with thin (red online) lines, while the ground-state potential of the N_2H^+ ion is shown with heavy black line. In (a) and (b) the potentials are displayed as functions of the z coordinate, while $r = 2.086a_0$ and $\theta = 1^\circ$, for resonant states of ${}^2A'$ and ${}^2A''$ symmetries, respectively. In (c) and (d), the potentials of ${}^2A'$ and ${}^2A''$ resonant states are displayed as functions of the angle θ when the two radial coordinates are fixed at $r = 2.086a_0$ and $z = 3.0a_0$. Finally, (e) and (f) show the r dependencies of the potentials when $z = 3.0a_0$ and $\theta = 1^\circ$.

surfaces were shown as functions of the the N-H bond length with an N-N distance of $2.1a_0$. In order to compare to their results, additional calculations in linear geometry are carried out to compute potentials of resonant states of 2A_1 symmetry, using this N-N bond distance. Since the calculations are done at different levels, all curves are referenced to

the ion at equilibrium geometry. The results are shown in Fig. 5.

The bottom figure shows a comparison of the current calculations with the adiabatic results of the group of Talbi and Hickman [16]. The calculated potential of the ionic ground state has an almost identical form as the one obtained by Talbi;

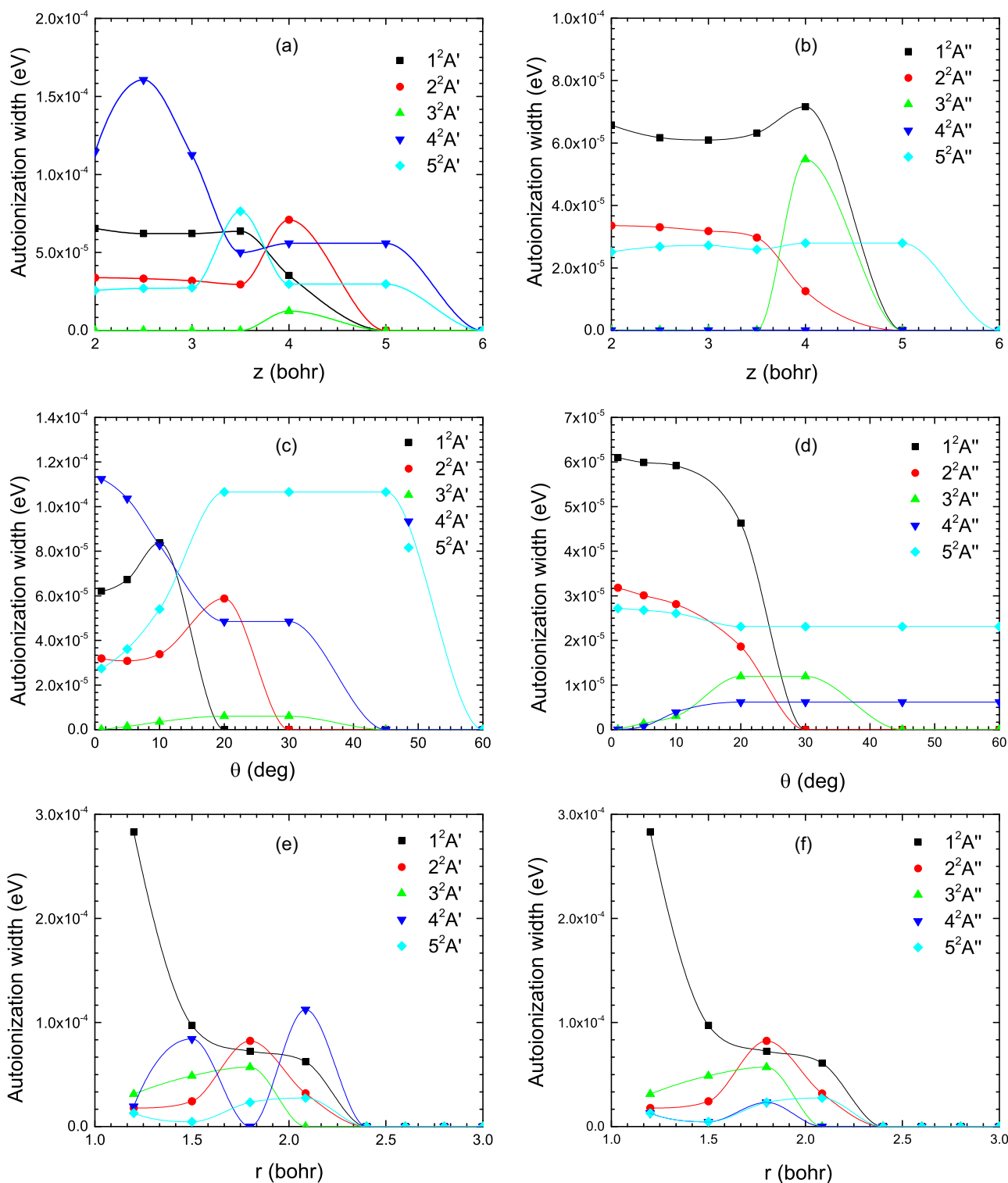


FIG. 4. Autoionization widths of the five lowest resonant states of $^2A'$ and $^2A''$ symmetries displayed in (a) and (b) as functions of the z coordinate, while $r = 2.086a_0$ and $\theta = 1^\circ$. In (c) and (d), the widths are shown as functions of the angle θ when the two radial coordinates are fixed at $r = 2.086a_0$ and $z = 3.0a_0$. Finally, (e) and (f) show the r dependencies of the widths when $z = 3.0a_0$ and $\theta = 1^\circ$.

and in the figure, the ion potential from present calculation is displayed with the heavy solid line. Our calculations, below the ion, in the Frank-Condon region agree well with those by Talbi. The current calculations include more Rydberg states, since the basis set included more diffuse basis function. At

larger internuclear separation the Talbi results are lower in energy, due to the larger calculation. Above the ion, the previous calculations show more states, but these include both resonance states and unphysical states having the character of a Rydberg lying above the parent ion. In the upper figure, the

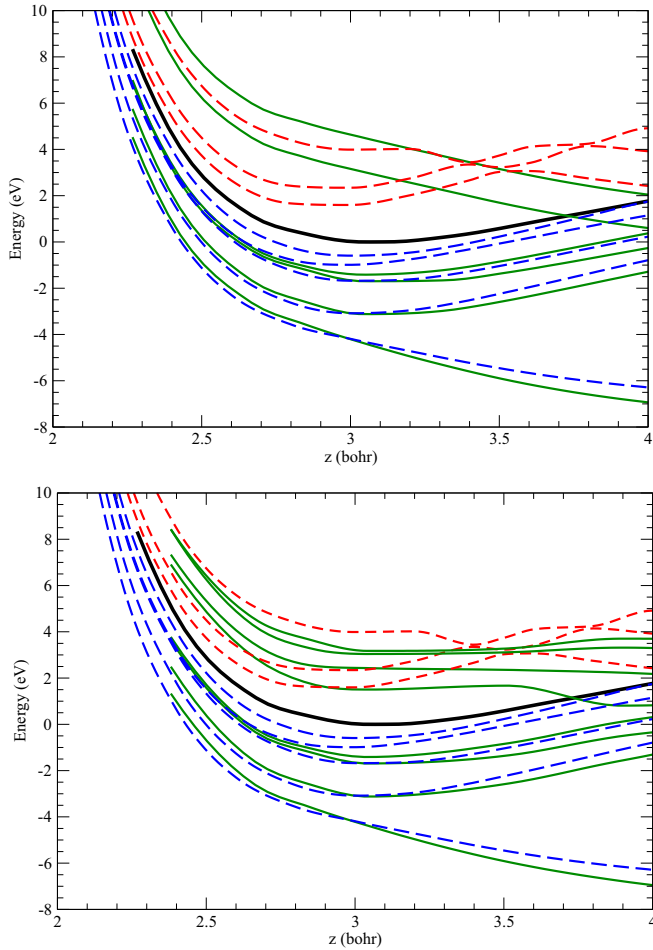


FIG. 5. Comparison to previous calculations, potentials of N_2H , top, diabatic, bottom, adiabatic displayed as functions of the z coordinate, while the NN distance $r = 2.1a_0$ and the angle $\theta = 0^\circ$ are frozen. The solid lines (green) are the results of the group of Talbi and Hickman [16]. The dashed lines are the resonant states from the current calculations, blue are Rydbergs, and red are resonant states. The ion curve is shown as a heavy solid line.

diabatic results of Talbi are shown. To produce these curves, Talbi *et al.* employed a procedure to remove these unphysical states. However, this procedure also eliminates Rydberg states converging to higher states of the ion, which lie below their parent and which are resonance states. It should also be noted that the fourth state in the previous calculations has a lower asymptote than our calculation. Since this correlates with the lower resonant state, this would result in a modified energy threshold for the dissociative recombination cross section. This will be further discussed in the following section where the calculated cross section is discussed.

B. DR cross section

The contribution to the DR cross section from direct electron capture into resonant states followed by dissociation is calculated using wave-packet propagation methods. No electronic couplings among neutral states are included. It is assumed that electron capture into the resonant states may either lead to autoionization or a direct dissociation.

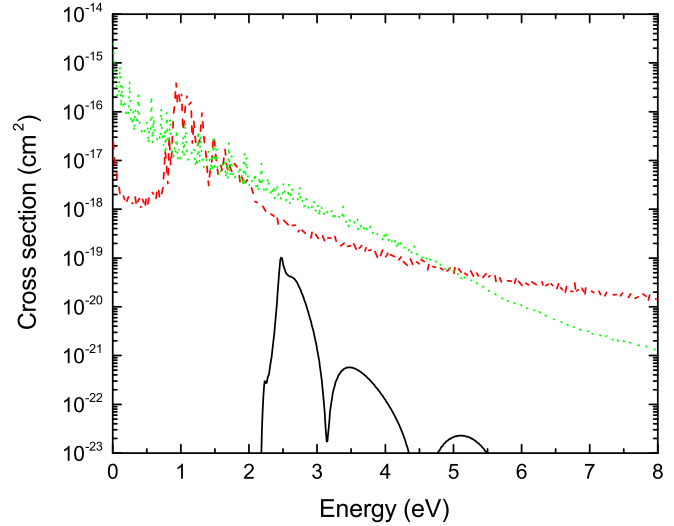


FIG. 6. Direct DR cross section through the lowest resonant state of $^2A'$ symmetry calculated using wave-packet propagation including one (solid black line), two (dashed red line), and three (dotted green line) degrees of freedom.

In Fig. 6, the direct DR cross section through the lowest resonant state of $^2A'$ symmetry is shown when the wave packet is propagated including one-, two-, and three degrees of freedom. In the one-dimensional (1D) calculation, only the Jacobi z coordinate is included, while $r = 2.086a_0$ and $\theta = 1^\circ$ are frozen. The 2D calculation includes z and θ , keeping $r = 2.086a_0$ fixed. The 1D calculation provides a threshold energy for dissociation of about 2.2 eV. The calculated DR cross section is significantly lower than those obtained when two or three degrees of freedom are considered. The 2D calculation produces a cross section with a peak around 0.7 eV. This is due to the fact that this energy is needed to capture into the resonant state. When the coordinate r is included, the electron can now be captured into the resonant states at lower collision energies. Calculated 3D cross section shows a E^{-1} dependence at low collision energies.

The direct DR cross section is calculated for the five lowest resonant states of $^2A'$ and $^2A''$ symmetries. The resulting cross sections are displayed in Fig. 7. The two lowest resonant states of each symmetry contribute to the DR cross section at low collision energies. Most important are the two lowest electronic states of $^2A'$ symmetry. These states are dissociating quasidiabatically into $N_2(^3\Sigma_u^+) + H$ and $N_2(^3\Pi_g) + H$.

As described above, the potentials of the resonant states calculated by the group of Talbi and Hickman [16] have lower asymptotic energies than the potential-energy surfaces considered here. In [16], a larger structure calculation was performed and we believe that when the resonant states have crossed the ion, their description of the resonant state is better than ours. To examine the effect on the direct DR cross section by a lowering of the asymptotic energy, we connect our potentials for the 1,2 $^2A'$ resonant states for $z \leq 3.0a_0$ with their potentials at larger values of z . For the θ and r dependencies, we used the form obtained in our calculations. The resulting cross sections for direct dissociation along modified potential-energy surfaces of the $1^2A'$ and $2^2A'$ resonant states are shown with the dashed lines in the top

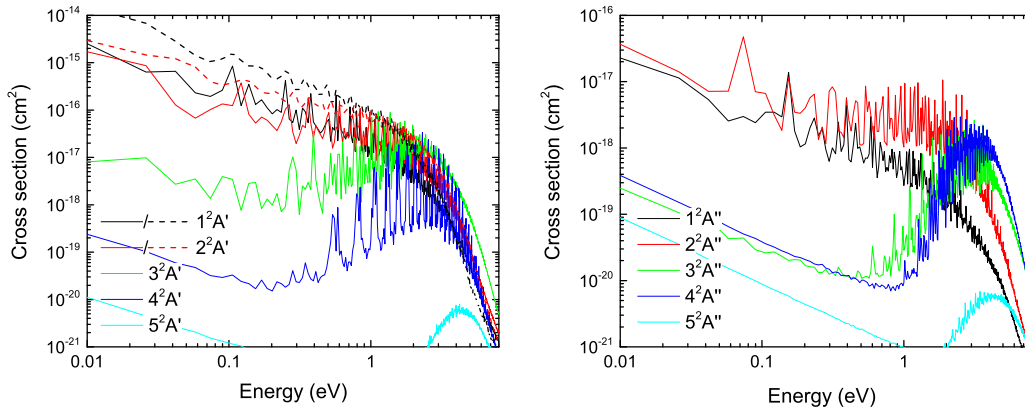


FIG. 7. Contributions from resonant states of $2^2A'$ (left) and $2^2A''$ (right) symmetries to the direct DR cross section of N_2H^+ calculated using wave-packet propagation including all three degrees of freedom. The dashed (black and red online) curves in the left figure show the cross section for wave-packet propagation on the modified potentials of the $1^2A'$ and $2^2A'$ resonant states, where the large z dependencies of the potentials are the same as what was obtained in the calculation by the group of Talbi and Hickman [16].

of Fig. 7. At low energies the direct DR cross section increases with as much as a factor of 10 for the $1^2A'$ resonant state.

In Fig. 8, we compare the measured cross section of DR of N_2H^+ using the CRYRING ion storage ring [13] with the calculated cross sections for the indirect and direct DR mechanisms.

For collision energies lower than 0.4 eV, the DR cross section calculated from the indirect mechanism dominates the cross section. As the threshold for each vibrational state is reached, the contribution from that state to the cross section (see Ref. [23]) goes to zero, leading to downward steps in the magnitude. At about 0.4 eV, only the contributions into the $v = 2$ modes are nonzero. At this point the direct DR cross section which at low energies is an order of magnitude smaller, now dominates the cross section. Overall, there is a good agreement between the calculated and measured cross section. In Fig. 7, we show the change in cross section that resulted from a shift in the asymptotic energies of the potential-energy curves. This change was significant only for low energies. However, in

that energy region, the total cross section is dominated by the indirect mechanism, so the overall effect is not significant.

V. CONCLUSION

Potential-energy surfaces and autoionization widths of resonant states important in N_2H^+ DR have been determined including all three nuclear degrees of freedom by combining electron-scattering calculations with structure calculations. The potential-energy surfaces have been compared with those calculated by the group of Talbi and Hickman [16].

The indirect and direct DR cross sections are calculated using simplified models. For the indirect mechanism, the cross section is obtained from a vibrational frame transformation of the elements of the scattering matrix obtained with the electron-scattering calculations. Autoionization is in this model and, contrary to Ref. [17], not only vibrational excitation of the ionic core of $v = 0$ to $v = 1$ are considered, but also $v = 0$ to $v = 2$. This extends the energy region, where the indirect mechanism contributes to the total cross section.

The direct DR cross section is computed by wave-packet propagation on three-dimensional potential-energy surfaces, where the 3D autoionization widths are considered. Our results clearly show that the indirect mechanism dominates at low collision energies, while the direct mechanism dominates at energies higher than 0.4 eV. We also find that the breakup proceeds almost entirely into the two-body ($\text{N}_2 + \text{H}$) channel with the three-body ($\text{N} + \text{N} + \text{H}$) as a minor channel. Further details on the branching ratios into specific N_2 electronic states would require inclusion of nonadiabatic couplings between the neutral states and are beyond the scope of this work.

ACKNOWLEDGMENTS

We are grateful to P. Hickman for providing us data of their potential-energy surfaces for comparison. We acknowledge support from the National Science Foundation under Grant No. PHY-11-60611 and the U.S. DOE Office of Basic Energy Science, Division of Chemical Science. Å.L. acknowledges support from the Swedish research council (Grant No. 2014-4164).

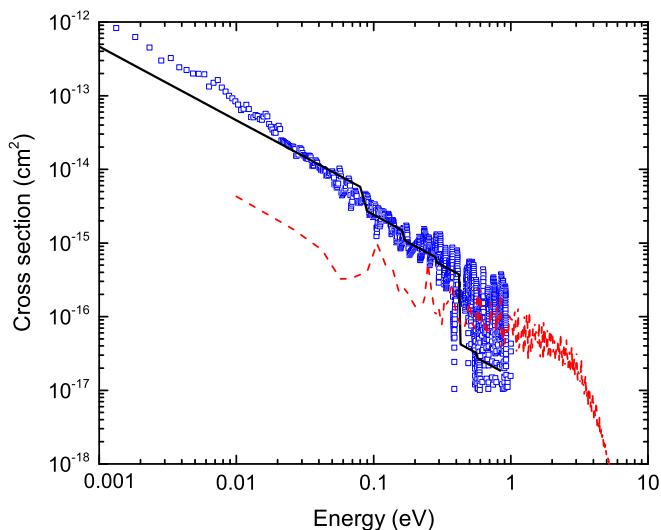


FIG. 8. Measured cross section of N_2H^+ DR (blue squares) [13] is compared with the calculated DR cross section through the indirect (black solid line) and direct (red dashed line) mechanisms.

- [1] B. E. Turner, *Astrophys. J.* **193**, L83 (1974).
- [2] A. Fuente, J. Martin-Pintado, J. Cernicharo, and R. Bachiller, *A&A* **276**, 473 (1993).
- [3] B. E. Turner, *Astrophys. J.* **449**, 635 (1995).
- [4] P. Caselli, C. M. Walmsley, A. Zucconi, M. Tafalla, L. Dore, and P. C. Myers, *Astrophys. J.* **565**, 331 (2002).
- [5] K. Tatematsu, *J. Korean Astron. Soc.* **38**, 279 (2005).
- [6] V. Vuitton, R. V. Yelle, and M. J. McEwan, *Icarus* **191**, 722 (2007).
- [7] D. Smith and N. G. Adams, *Astrophys. J.* **284**, L13 (1984).
- [8] N. G. Adams, C. R. Herd, M. Geoghegan, D. Smith, A. Canosa, J. C. Gomet, B. R. Rowe, J. L. Queffelec, and M. Moriais, *J. Chem. Phys.* **94**, 4852 (1991).
- [9] W. D. Geppert, R. Thomas, J. Semaniak, A. Ehlerding, T. J. Millar, F. Österdahl, M. af Ugglas, N. Djurić, A. Paál, and M. Larsson, *Astrophys. J.* **609**, 459 (2004).
- [10] V. Poterya, J. L. McLain, N. G. Adams, and L. M. Babcock, *J. Phys. Chem. A* **109**, 7181 (2005).
- [11] C. D. Molek, J. L. McLain, V. Poterya, and N. G. Adams, *J. Phys. Chem.* **111**, 6760 (2007).
- [12] P. A. Lawson, D. Osborne Jr., and N. G. Adams, *Int. J. Mass Spectrom.* **304**, 41 (2011).
- [13] E. Vigren, V. Zhaunerchyk, M. Hamberg, M. Kaminska, J. Semaniak, M. af Ugglas, M. Larsson, R. D. Thomas, and W. D. Geppert, *Astrophys. J.* **757**, 34 (2012).
- [14] D. Talbi, *Chem. Phys.* **332**, 298 (2007).
- [15] A. P. Hickman, D. O. Kashinski, R. F. Malenda, F. Gatti, and D. Talbi, *J. Phys. Conf. Ser.* **300**, 012016 (2011).
- [16] D. O. Kashinski, D. Talbi, and A. P. Hickman, *Chem. Phys. Lett.* **529**, 10 (2012).
- [17] S. Fonseca dos Santos, N. Douguet, V. Kokoouline, and A. E. Orel, *J. Chem. Phys.* **140**, 164308 (2014).
- [18] D. O. Kashinski, D. Talbi, and A. P. Hickman, *EPJ Web Conf.* **84**, 03003 (2015).
- [19] T. Pacher, L. S. Cederbaum, and H. Köppel, *J. Chem. Phys.* **89**, 7367 (1988).
- [20] G. A. Worth, M. H. Beck, A. Jäckle, and H.-D. Meyer, The MCTDH Package, Version 8.4, University of Heidelberg, Germany, 2007, see <http://mctdh.uni-hd.de>.
- [21] T. N. Rescigno, C. W. McCurdy, A. E. Orel, and B. H. Lengsfeld III, The Complex Kohn Variational Method, in *Computational Methods for Electron-molecule Scattering*, edited by W. H. Huo and F. A. Gianturco (Plenum, New York, 1995).
- [22] C. Jungen and S. T. Pratt, *Phys. Rev. Lett.* **102**, 023201 (2009).
- [23] N. Douguet, A. E. Orel, C. H. Greene, and V. Kokoouline, *Phys. Rev. Lett.* **108**, 023202 (2012).
- [24] C. W. McCurdy and J. L. Turner, *J. Chem. Phys.* **78**, 6773 (1983).
- [25] A. E. Orel, *Phys. Rev. A* **62**, 020701(R) (2000).
- [26] A. Jäckle and H.-D. Meyer, *J. Chem. Phys.* **105**, 6778 (1996).
- [27] S. Geltman, *Topics in Atomic Collision Theory* (Academic Press, New York, 1997), p. 31.
- [28] M. H. Beck, A. Jäckle, G. A. Worth, and H.-D. Meyer, *Phys. Rep.* **324**, 1 (2000).